coatings

MDPI

Article

Dyes amount and light Scattering Influence on the Photocurrent Enhancement of Titanium Dioxide Hierarchically Structured Photoanodes for Dye-Sensitized Solar Cells

Wen-Yao Huang [1] and Tung-Li Hsieh [2,*]

[1] Department of Photonics, National Sun Yat-sen University, 70 Lienhai Road, Kaohsiung 80424, Taiwan; wyhuang@faculty.nsysu.edu.tw

[2] General Education Center of Wenzao Ursuline University of Languages, 900 Mintsu, 1st Road, Kaohsiung 80793, Taiwan

* Correspondence: tunglihsieh@gmail.com; Tel.: +886-7-342-6031#7226

Received: 28 October 2019; Accepted: 20 December 2019; Published: date

Abstract: In this study, we prepared and analyzed the properties of hill-like hierarchically structured titanium dioxide (TiO_2) photoanodes for dye-sensitized solar cells (DSSCs). We expected that the presence of appropriately aggregated TiO_2 clusters in the photoanode layer would translate to relatively strong light scattering and dye loading, increasing the photovoltaic efficiency. A detailed light-harvesting study was performed by employing polyvinyl alcohol (PVA) polymers of different molecular weights as binders for the aggregation of the TiO_2 nanoparticles (P-25 Degussa). Hence, we obtained a series of TiO_2 films, presenting a variety of morphologies. Their reflection, as well as absorbance of light by the attached dye, the amount of dye loading, and the performance of the fabricated DSSC devices were investigated. Our optimized device, with a relatively high dye loading and good light harvesting ability, was able to enhance the short-circuit current (J_{sc}) in the DSSCs by 23%.

Keywords: hierarchical structure; TiO_2 photoanode; dye-sensitized solar cell; light scattering

1. Introduction

Recently, dye-sensitized solar cells (DSSCs) have attracted significant attention [1–9] because of their low production cost and high conversion efficiency. In general, the photoanode of a DSSC is represented by a porous layer, as follows: 20 nm TiO_2 particles are coated on a transparent conductive oxide (TCO) glass, and a monolayer of a charge transfer dye is applied to the porous film. Under illumination, the dye molecules become photoexcited and release electrons; these are injected into the conduction band of TiO_2, diffuse through the porous layer, and are subsequently collected and transported to the external load by the TCO. Porous TiO_2 electrodes play an important role in improving the performance of DSSCs. In fact, these devices should ideally possess a TiO_2 layer with a high surface area, allowing for a large adsorption area and good light scattering. These properties translate into enhanced light harvesting, short-circuit current (J_{sc}), and power conversion efficiency [10]. The research results of Wang et al. [11] demonstrated an obvious decrease of the surface area in association with an increase in particle size. These authors indicated that the use of very small TiO_2 particles was essential to increase the surface area of the TiO_2 layer and to increase the amount of dye, while large particles were required to enhance the absorption of red light through light scattering. A simultaneous increase of the surface area and of light scattering is not possible, as these two properties oppose each other. Previous studies have indicated that the aggregation of TiO_2

nanoparticles in a hierarchical structure can improve the performance of DSSCs [12,13]. Moreover, these structured TiO_2 films were found to improve the efficiency of electrolyte diffusion or penetration, presenting high dye loadings and enhancing the scattering effect. However, the influence of the amount of dye and its light scattering effect on light harvesting have not been discussed in detail. Yet, on the other hand, the presence of a macrostructure might prevent effective dye loading onto the electrode [14].

The Mie theory entails that the intensity of light scattering depends on the size of the illuminated object: the scattering cross-section increases with the size of the scattering object. This theory has been conveniently applied to light harvesting in solar cells [15], especially for longer wavelengths [16–18]. In our study, we aimed to obtain a film characterized by both a high surface area and good light scattering. In order to evaluate the balance between these two factors and their influence on light harvesting, we created a series of hierarchically structured TiO_2 films with different degrees of aggregation (Figure 1). In order to perform a detailed light harvesting study, we employed polyvinyl alcohol (PVA) polymers of different molecular weights as binders for the aggregation of TiO_2 nanoparticles. Hence, we obtained a series of TiO_2 films presenting a variety of morphologies. Their reflection, as well as the absorbance of the attached dye, the amount of dye loading, and the performance of the fabricated DSSC devices, were investigated. Finally, we created an optimized device characterized by a relatively high dye loading and good light harvesting ability, and were able to enhance the short-circuit current (J_{sc}) in the DSSCs by 23%.

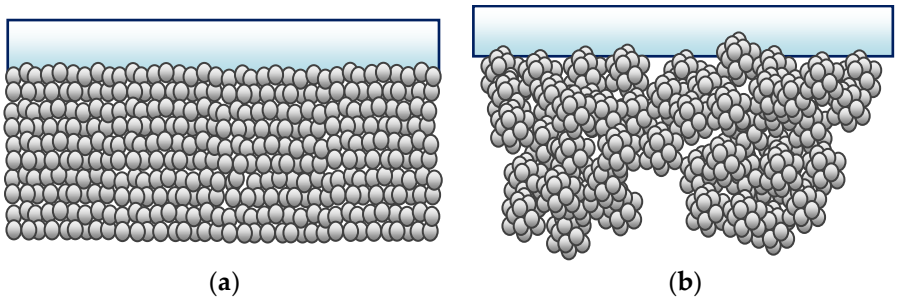

Figure 1. Schematic diagram of (**a**) conventional film and (**b**) hierarchical structured film.

2. Experimental Design

2.1. Preparation of a Hierarchically Structured TiO_2 Particle Paste

A hierarchically structured TiO_2 paste was prepared using PVA (CCP) as the binder to aggregate the TiO_2 nanoparticles. The size of the aggregations was regulated by altering the molecular weight (MW = 31,000–99,000) of the polymers. First, 1 g of a PVA–water solution was stirred at 65 °C overnight and dissolved in a mixed solvent (1.0 mL H_2O + 0.8 mL ethanol). Then, 0.6 g of TiO_2 powder (P-25, 21 nm Degussa) was added to the solution. The resulting suspension was placed in an ultrasonic cleaner for 30 min. After 0.05 mL of Triton X-100 and 0.05 mL of acetyl-acetone surfactants were added to the suspension, it was placed again in the ultrasonic cleaner for 30 min, and then stirred for 24 h.

2.2. Fabrication of the DSSCs

A dense TiO_2 layer of about 45 nm was spin-coated on an indium tin oxide (ITO) glass (Merck), which was used as a blocking layer to avoid recombination due to I_3^- grabbing photoelectrons on the conducting substrate surface. A TiO_2 porous layer, with an active area of 1.3 × 0.8 cm^2, was formed through this spin-coating process. To induce the evaporation of the solvent, the decomposition of the PVA, and to ensure the electrical contact and mechanical adhesion of the TiO_2 films on the glass, these were baked at 100 °C for 10 min, and subsequently calcined at 450 °C for ~30 min in the presence of air. The average thickness of the TiO_2 films (~10 μm) was checked using an α-step surface profiler. Dye adsorption was achieved by immersing the calcined films in a 5×10^{-4} M ruthenium dye solution,

cis-bis(isothiocyanato) bis(2,2′-bipyridyl-4,4′-dicarboxylato) ruthenium(II) bis-tetrabutylammonium (D719 dye, Eversolar), and in a tert-butanol and acetonitrile co-solvent, for 20 h at 25 °C. The dye adsorbed on the TiO_2 films was rinsed with ethanol and dried at 85 °C for 10 min. Pt-coated ITO was used as a counter electrode; subsequently, the dye-adsorbed TiO_2 films were sealed using a hot-melt adhesive (thickness = 30 μm, Surlyn, Tripod). A liquid electrolyte consisting of I_2 (0.1 M), LiI (0.1 M), 1-propyl-2,3-dimethylimidazolium iodide (DMPII; 0.6 M), and 4-tert-butylpyridine (TBP; 0.25 M, Aldrich) in 3-Methoxypropionitrile (MPN; Fluka) was then injected to fill the space between the cells.

For the sake of comparison, we also prepared a conventional TiO_2 film (without the addition of PVA); the device as a standard was fabricated using the same methods as those described above.

2.3. Characterization and Measurement

The surface morphology of the TiO_2 porous films was observed by field-emission gun-scanning electron microscopy (JEOL JSM-6700F). The reflectance and absorbance spectra were measured by a UV-VIS spectrometer (Perkin Elmer UV-Vis Lambda35). The photocurrent-voltage of the DSSC was measured using a Keithley 2400 analyzer under AM 1.5 simulated illuminations, with an intensity of 100 mW/cm^2. A 300 W xenon lamp (MODEL 6258) was used as the light source—a filter was applied to approximate the sunlight spectrum. The incident photo-to-current conversion efficiency (IPCE) spectra were measured by a self-designed IPCE system, consisting of a xenon lamp (Xe Light source 70051), a monochromator (Cornerstone 13074004), a power measurement (2935-C), a source measurement unit (M3500A), and a power detector (818-SL).

The level of dye adsorption was evaluated by the following method: the dye molecules were desorbed from the TiO_2 layer by rinsing it with a 0.1 M NaOH [19,20] aqueous solution; then, the absorbance at 511 nm of the dye solution was measured by UV-VIS spectrometry, determining its concentration.

3. Results and Discussion

3.1. Morphologies of the TiO_2 Films

In order to determine the optical properties of the TiO_2 films characterized by different degrees of particle aggregation, we used PVA with different molecular weights as binders. These films were expected to present different levels of light reflectance and absorbance, as well as dissimilar morphologies. To verify the presence of aggregations in the paste, we diluted the paste and observed it by SEM (Figure 2). These observations confirmed the presence of numerous micro-aggregations composed of TiO_2 nanoparticles; moreover, the sizes of these aggregations tended to increase with the molecular weights of the PVAs used. We supposed that, in each sample, the interactions between the PVA, the TiO_2 particles, and the surfactant were in a state of static equilibrium. In these stable conditions, numerous uniformly-sized TiO_2 aggregations occurred in the paste; additionally, the relationship between their size and the molecular weight of the PVA was derived from the interaction between TiO_2 and PVA. In order to investigate the aggregation mechanism, we maintained the same molecular weight, while changing the amount of PVA from 0.2 g to 0.3 g (Figure 3). Despite this change, the size of the aggregations did not vary. Probably, the hydroxyl groups contained in the PVA molecules interacted with those on the TiO_2 particles, forming clusters in the processing paste. These TiO_2–PVA clusters did not aggregate continuously, because of the influence of the surfactant. When the PVA molecular weight increased, the number of hydroxyl groups in each PVA molecule increased as well—the interaction between the PVA molecules and the TiO_2 particles became stronger, inducing the formation of bigger aggregations in the paste. When a greater amount of PVA molecules were added to the paste, however, the number of hydroxyl groups in each PVA molecule did not change—the addition of PVA did not cause an enlargement of the aggregations, but just increased their number.

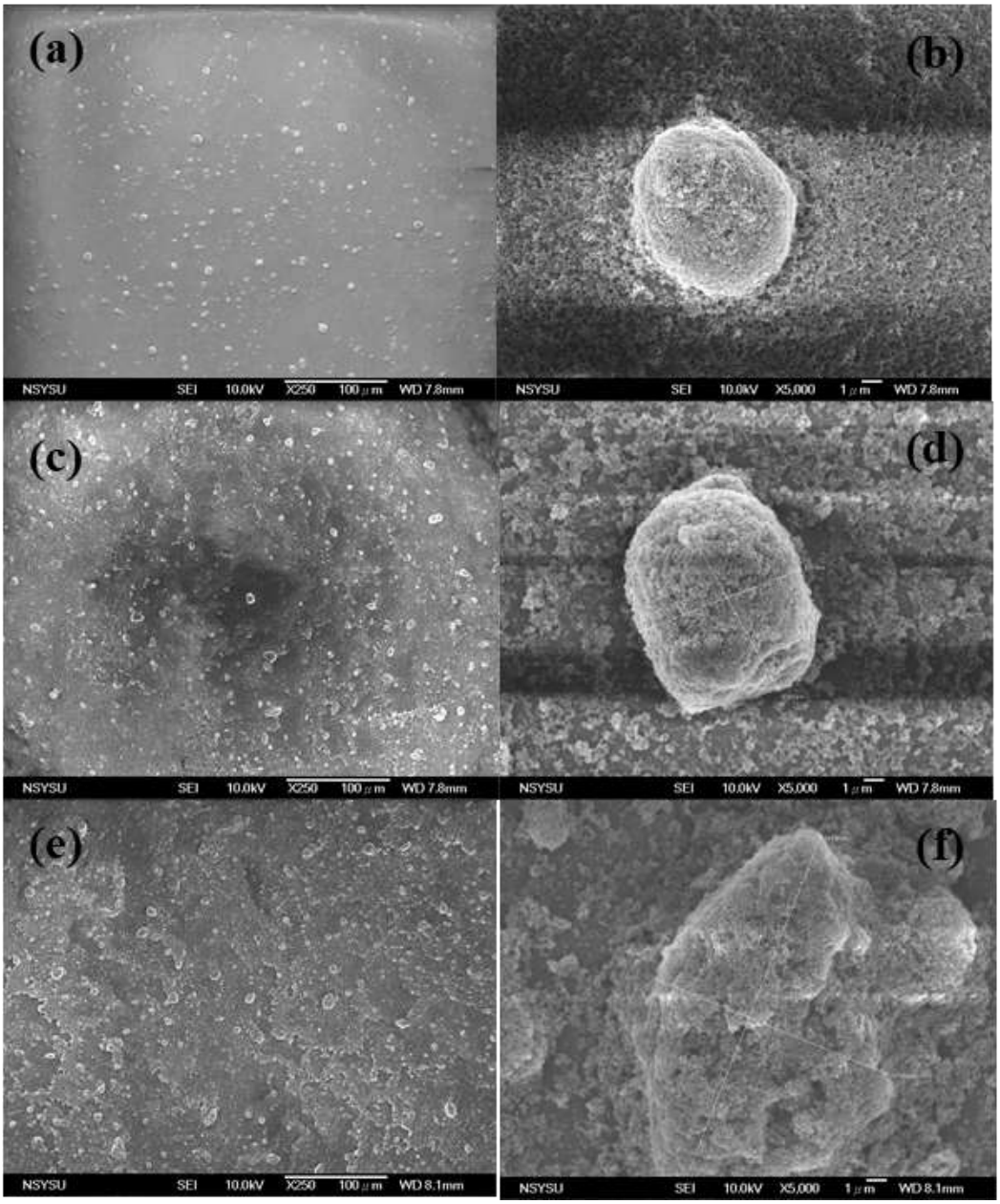

Figure 2. SEM images of TiO_2 aggregations from diluted paste: (**a**,**b**) 31,000 molecular weight (MW); (**c**,**d**) 40,000 MW; (**e**,**f**) 54,000 MW.

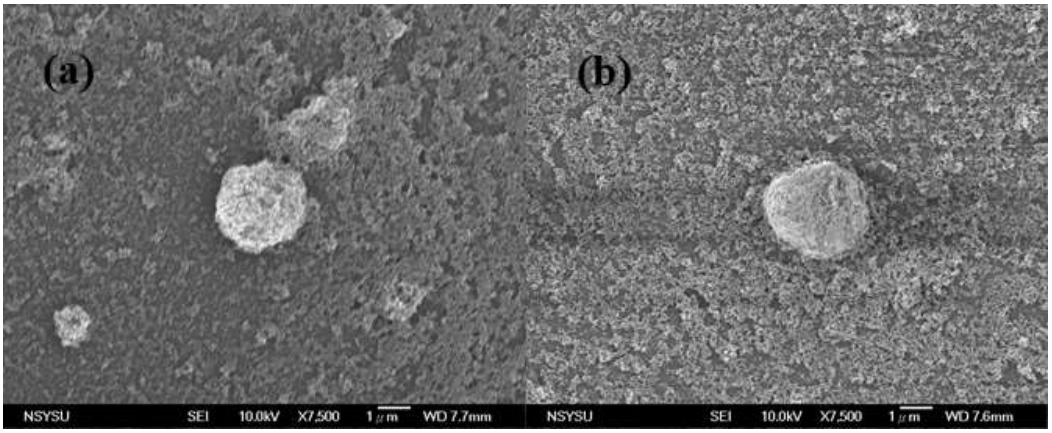

Figure 3. SEM images of TiO_2 aggregations from diluted paste with polyvinyl alcohol (PVA): (**a**) 0.2 g; (**b**) 0.3 g.

Figure 4 shows the surface (SEM) images of both the conventional and PVA-treated films. The conventional film was created by uniformly stacking the nanoparticles. The size of the TiO_2 aggregations and the porosity of this film were proportional to the molecular weight of the PVA used. From Film A to Film D, the size of the aggregations increased from ~100 nm to 300 nm. These results suggest that the use of PVAs with higher molecular weights induced the formation of larger TiO_2–PVA aggregations in the paste. Relatively big TiO_2 aggregations persisted after coating the substrate and following polymer decomposition (during the calcining process). The side views observed by the SEM (Figure 5) revealed that the conventional film possessed a very smooth top surface, while the surfaces of the PVA-treated films were hill-like (probably due to the occurrence of TiO_2 micro-clusters). The presence of these micro-/nano-aggregations in the hierarchically structured TiO_2 film suggested that such a structure would provide an enhanced light scattering effect.

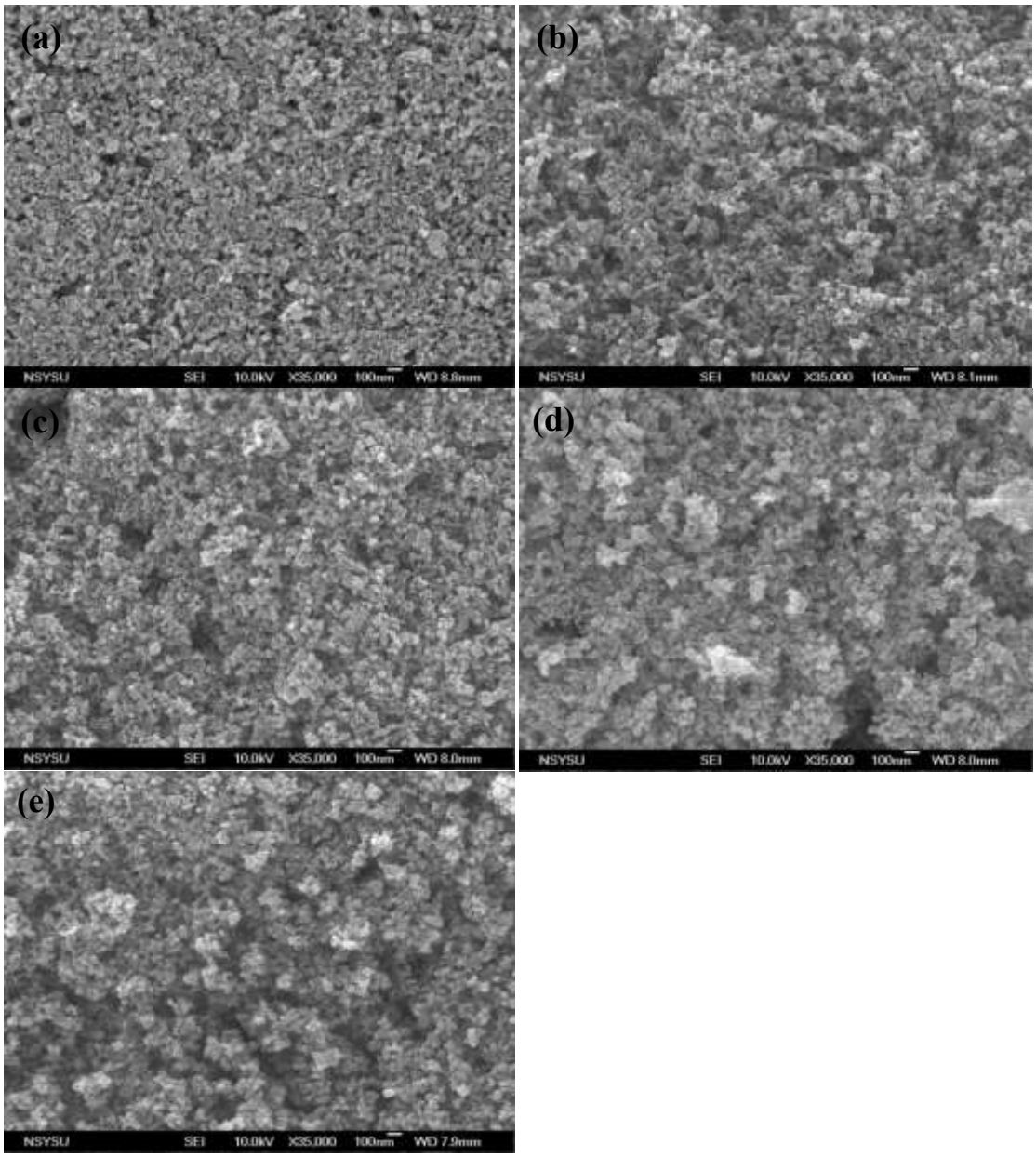

Figure 4. Surface SEM images of (**a**) conventional TiO_2 film, PVA-treated TiO_2 films with (**b**) 31,000 MW, (**c**) 40,000 MW, (**d**) 54,000 MW, and (**e**) 99,000 MW.

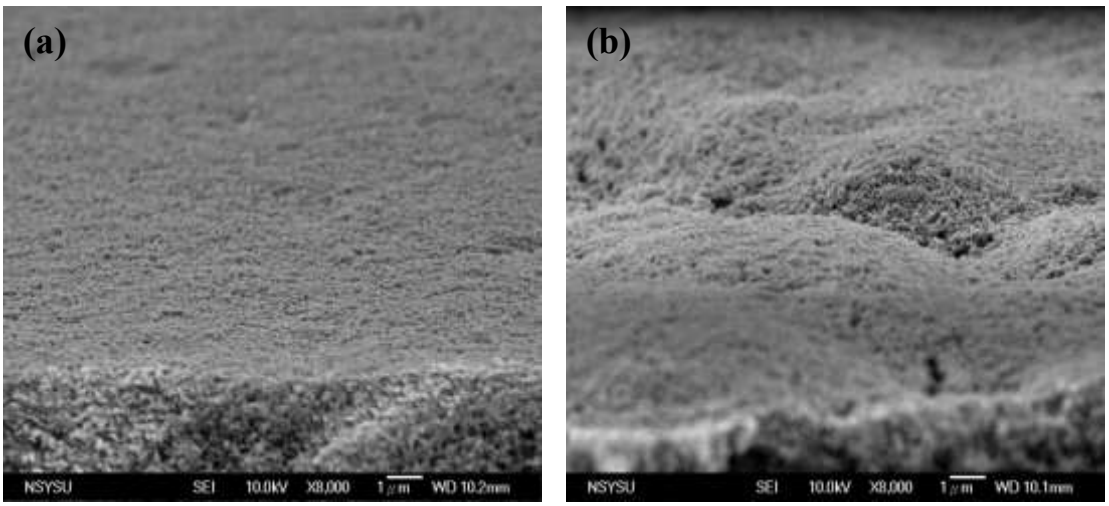

Figure 5. Side view SEM images of (**a**) conventional TiO_2 film and (**b**) PVA-treated TiO_2 film.

3.2. Optical Properties of TiO_2 Films and Photoanodes

To determine the light scattering effects of the TiO_2 films, we measured their reflectance (Figure 6a). The reflectance of standard (STD) was lower than that of the others, as its uniformly stacked nanoparticles were not able to scatter the incident light efficiently. The PVA-treated films on the other hand, in which the nanoparticles were aggregated, forming a hierarchically structured film, provided a higher reflectance. Additionally, the normalized reflectance spectra (Figure 6b) showed some differences. An analysis of the longer wavelength regions in each curve (600–800 nm) indicated that the size of the aggregations in the samples increased with the reflectance. This phenomenon is in accordance with the Mie scattering theory. Our data (Figure 6) show that the molecular weight had an influence on the size of the aggregated particles, thus causing a different scattering or reflection of the hierarchically structured photoanodes, which was particularly significant when the molecular weight was 99,000. However, it is impossible to conclusively confirm this with the limited data. Figure 6a shows the results when the TiO_2 films were not normalized; the higher the molecular weight of the PVA added to each film, the greater the reflectivity and the stronger the scattering effect. In contrast, Figure 6b shows the results after the normalization treatment of the TiO_2 films. There was no significant difference among the films at short wavelengths; however, it can be clearly seen at long wavelengths that when a PVA with high molecular weight was added, the film reflectivity was increased. Therefore, we can infer that the addition of the PVA with a high molecular weight increases the aggregation effect, which increases the scattering and reflectivity of the hierarchically structured photoanodes. The Mie theory entails that when the magnitude of particle aggregation is the same as the wavelength, the scattering effect or refraction appears to be the largest.

So far, several studies have discussed the light reflectance related to the scattering effect of TiO_2 films [17,21]. However, we could not determine how the reflected photons were scattered in the porous films. The incident light was scattered by the nanoparticles, and subsequently reflected forward or transversely through the porous film; by measuring only the reflectance, we actually neglected the photons scattered towards and through the film. Moreover, it is technically difficult to place a detector in the film for the measurement of the scattering intensity. In this study, the light scattering effect was investigated thoroughly by measuring the unit of dye absorbance. Our objective was to understand how much light was actually absorbed in the film by each dye molecule, as well as to characterize the intensity of the light scattering effect. The absorbance spectra of the dye molecules in the TiO_2 films are shown in Figure 7. These spectra were obtained by deducting the absorbance of the TiO_2 films from the photoanodes (i.e., TiO_2 with dye), and then eliminating the amount of dye on each film. Figure 8 clearly shows that each unit of dye molecules was able to harvest more light in the PVA-treated films, and that the light absorbance of each dye increased with the size of the aggregations. These results indicate that the light scattering effect was significantly stronger in the films containing bigger aggregations.

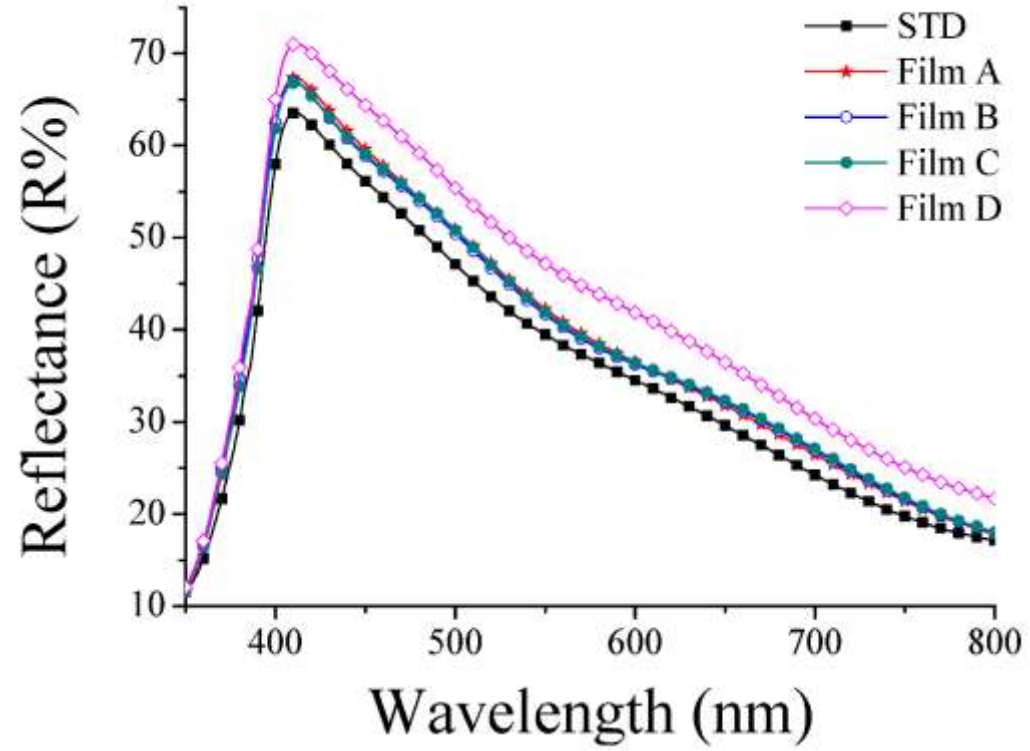

(**a**)

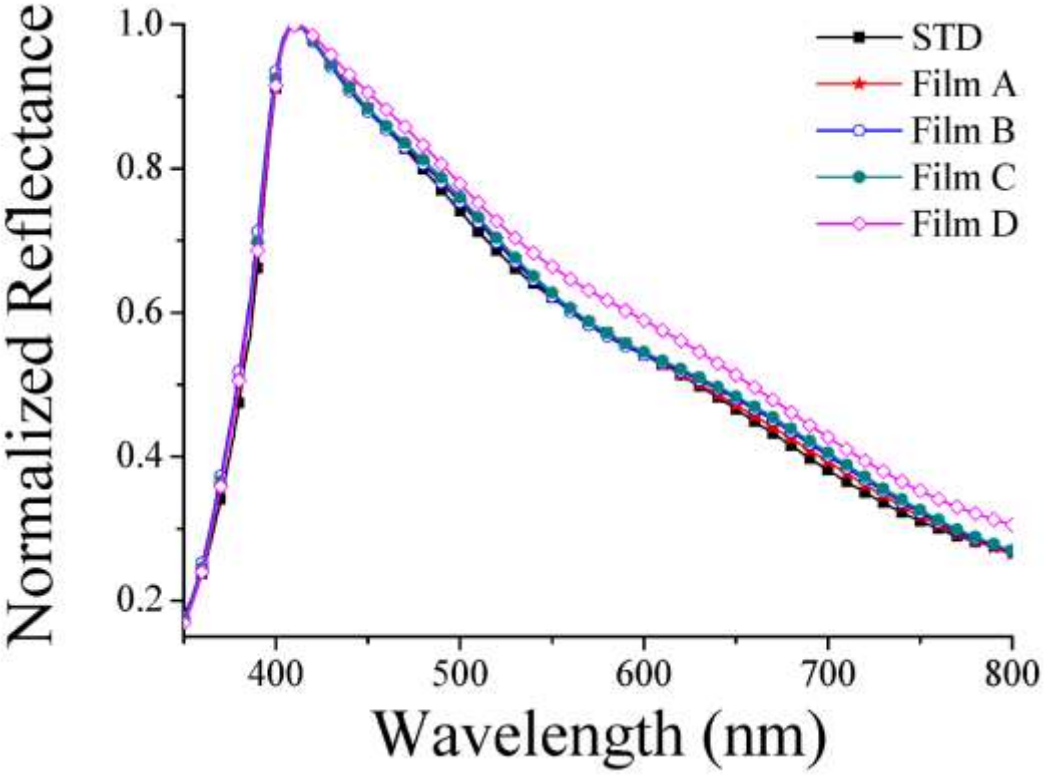

(**b**)

Figure 6. (**a**) Reflectance spectra of TiO_2 films. (**b**) Normalized reflectance spectra of TiO_2 films.

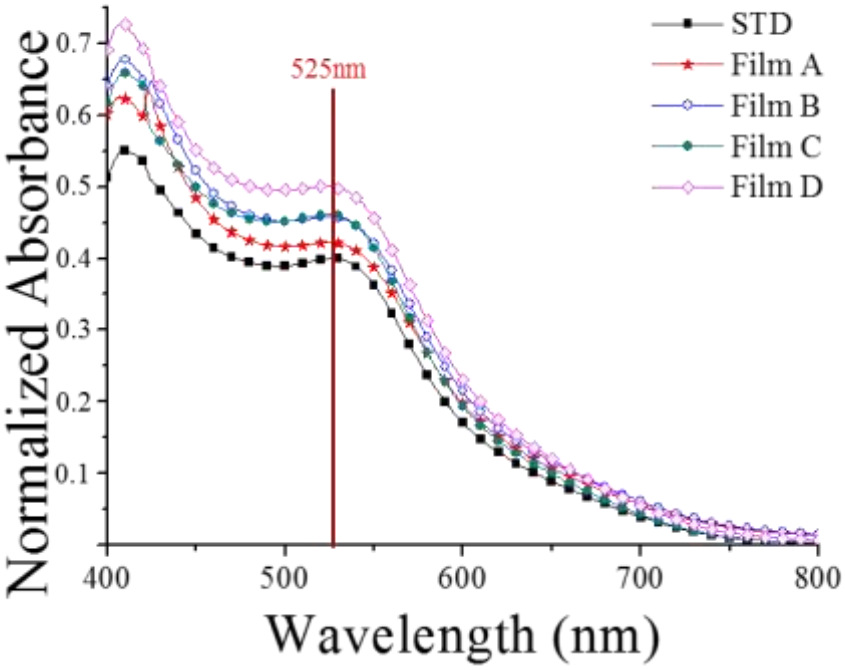

Figure 7. Absorbance spectra of each dye molecule in the TiO_2 films.

3.3. Performances of the DSSCs

As Figure 7 shows the scattering effect of each device after normalization for the absorbed dye amount of each device, and Figure 8 shows the results of combining the absorbed dye amount and the scattering effect of the hierarchically structured photoanodes of devices, the results are presented differently in these figures. The optical properties of the TiO_2 films with different morphologies have been described in the previous section. Here, we will discuss the performance of the devices in relation to light scattering, which is summarized in Table 1. Table 1 shows that a notable trend of comparison was observed in the photoelectric conversion efficiency (η) and short-circuit current (J_{sc}). Moreover, the relatively large aggregated TiO_2 of Film D resulted in a relatively high porosity and larger pores. This explains Film D's adequate reflectance, even when its quantum efficiency in a relatively short wavelength region was lower than that of other films. Devices A to D were fabricated using different TiO_2 films (A to D). We noticed that when the size of the aggregations increased, the dye amount decreased. This effect was probably linked to the change in surface area—the scattering effect should have increased, reflecting the occurrence of larger aggregations. The short-circuit current did not decrease directly from Device A to D. In fact, based on the analyses of Device C, we identified a turning point in the balance between the amount of dye and the light scattering effect. Moreover, although Film D possessed a lower amount of dye at 5.81×10^{-8} mol/cm^2 than the conventional film at 6.35×10^{-8} mol/cm^2, the short-circuit and power conversion efficiency of Device D were lower than those of the STD device (made using conventional film). These results suggested that the light scattering had a stronger influence than the dye amount on the performance of Device D. The same conclusions could be derived from the IPCE spectra (Figure 8), namely: the quantum efficiencies of the STD and A and D Devices were all maximized to ~550 nm after the application of the D719 dye. The peak quantum efficiency of Device D was almost equal to that of the STD device, but it was higher within the longer wavelength region (between ~560–700 nm). The higher efficiency in this spectral region could have been linked to a stronger scattering effect, induced by the formation of bigger TiO_2 aggregations. As Device A possessed the highest amount of dye and the best scattering effect, it also presented the highest quantum efficiency over the whole spectral range, the highest power conversion efficiency (4.47%), and a 23% increase in J_{sc} compared to the STD device.

In addition, the quantum efficiency of Device D in the shorter wavelength region of the IPCE spectrum was lower than that of the other devices. This may have been due to the higher porosity and bigger pores of Film D, derived from the larger size of its TiO_2 aggregations. When light was incident on the film, the longer wavelengths were well scattered, but the shorter wavelengths were perhaps not properly scattered because of the high structural porosity of the film itself. However, the photons deriving from the shorter wavelength regions could have been reflected forward as a result of the relatively high thickness of the film—there were enough chances for it to be reflected. Such a mechanism would explain why Device D presented a lower quantum efficiency, but not a lower reflectance than other films in the shorter wavelength region.

Table 1. Performance of dye-sensitized solar cells (DSSCs).

Sample	Adsorbed Dye ($\times 10^{-8}$ mol/cm^2)	Scattering Effect (525 nm) [a]	J_{sc} (mA/cm^2)	V_{oc} (V)	FF	η (%)
STD	6.35	weakest	10.63	0.58	0.69	4.08
Device A	6.46	weak	11.65	0.59	0.65	4.47
Device B	5.92	middle	9.41	0.59	0.65	3.64
Device C	5.56	strong	9.49	0.57	0.68	3.71
Device D	5.81	strongest	9.50	0.58	0.66	3.79

Note [a]: represents a comparison of the corresponding scattering effect in Figure 7 at a wavelength of 525 nm, where a large value indicates a strong scattering effect. STD—standard.

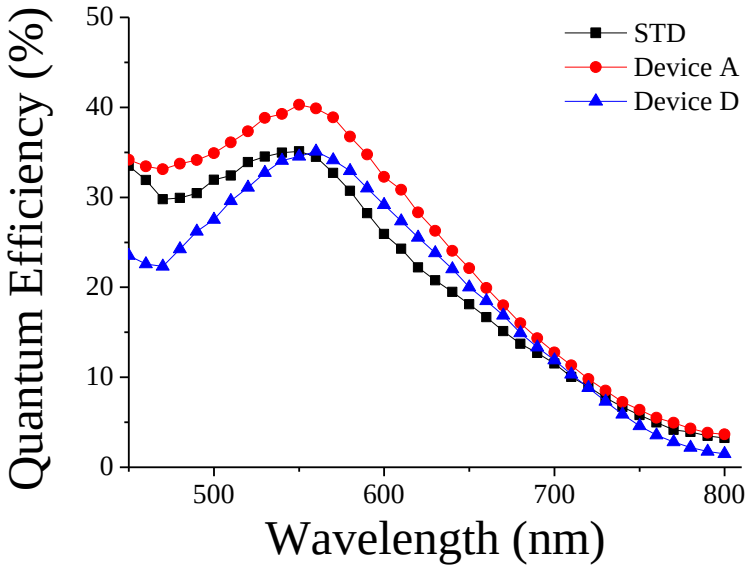

Figure 8. Incident photo to current conversion efficiency spectra of DSSCs.

4. Conclusions

The results shown in Figure 7 were due to the fact that each device was normalized for the absorbed dye amount in order to eliminate the effect of the absorbed dye amount, and the absorbed dye amount per unit area of each device was different due to the different degree of particle aggregation within each device. Thus, the degree of scattering for each device could not be accurately determined. Therefore, each device should first be normalized for the absorbed dye amount, and divided by the absorbed dye amount per unit area of each device. Hence, Figure 7 shows that the curve of STD was the lowest, while the curve of device D was the highest. Furthermore, the magnitude of the scattering effect of each device, after normalization for the absorbed dye amount, can be observed. The device efficiency was mainly determined by the absorbed dye amount, followed by the influence of the hierarchically structured scattering effect. Although we can infer from Figure

7 that the degree of particle aggregation contributed to the hierarchically structured scattering effect, it was not conducive to the absorbed dye amount; thus, we need to study the optimal conditions for the devices [22]. In this study, we prepared and characterized a series of hierarchically structured TiO_2 photoanodes. The analyses indicated that J_{sc} tended to increase with the scattering effect in the films characterized by increasingly larger TiO_2 aggregations. In our study, higher J_{sc} values corresponded to more efficient light scattering in the photoanodes, although the dye absorption decreased. The optimized Device A, created using a PVA (31,000 MW)-treated film, presented the highest dye loading and best light harvesting (resulting in a 23% increase of the J_{sc}), and the optimum power conversion efficiency (4.47%).

Author Contributions: T.-L.H. and W.-Y.H. conceived of the presented idea. T.-L.H. developed the theory and performed the computations. T.-L.H. verified the analytical methods. W.-Y.H. was encouraged to investigate a specific aspect and supervised the findings of this work. All of the authors discussed the results and contributed to the final manuscript.

Funding: This research received no external funding.

Acknowledgments: This research has been reviewed by the committee of IEEE ECICE 2019 and is recommended to be submitted to the SCI journal *Coatings*.

Conflicts of Interest: The authors declare no conflict of interest.

References

1. O'Regan, B.; Grätzel, M. A low-cost, high-efficiency solar cell based on dye-seneitized colloidal TiO_2 films. *Nature* **1991**, *353*, 737–740.
2. Grätzel, M. Dye-sensitized solar cells. *J. Photochem. Photobiol.* **2003**, *4*, 145–153.
3. Lee, K.-M.; Suryanarayanan, V.; Ho, K.-C. A study on the electron transport properties of TiO_2 electrodes in dye-sensitized solar cells. *Sol. Energy Mater. Sol. Cells* **2007**, *91*, 1416–1420.
4. Hu, L.; Dai, S.; Weng, J.; Xiao, S.; Sui, Y.; Huang, Y.; Chen, S.; Kong, F.; Pan, X.; Liang, L.; et al. Microstructure design of nanoporous TiO_2 photoelectrodes for dye-sensitized solar cell modules. *J. Phys. Chem.* **2007**, *111*, 358–362.
5. Varghese, O.K.; Paulose, M.; Grimes, C.A. Long vertically aligned titania nanotubes on transparent conducting oxide for highly efficient solar cells. *Nat. Nanotechnol.* **2009**, *4*, 592–597.
6. Qian, J.; Liu, P.; Xiao, Y.; Jiang, Y.; Cao, U.; Ai, X.; Yang, H. TiO_2-coated multilayered SnO_2 hollow microspheres for dye-sensitized solar cells. *Adv. Mater.* **2009**, *21*, 3663–3667.
7. Yu, H.; Zhang, S.; Zhao, H.; Xue, B.; Liu, P.; Will, G. High-performance TiO_2 photoanode with an efficient electron transport network for dye-sensitized solar cells. *J. Phys. Chem.* **2009**, *113*, 16277–16282.
8. Grätzel, M. Recent advances in sensitized mesoscopic solar cells. *Acc. Chem. Res.* **2009**, *42*, 1788–1798.
9. Yu, J.; Fan, J.; Zhao, L. Dye-sensitized solar cells based on hollow anatase TiO_2 spheres prepared by self-transformation method. *Electrochim. Acta* **2010**, *55*, 597–602.
10. Krašovec, U.O.; Berginc, M.; Hočevar, M.; Topič, M. Unique TiO_2 paste for high efficiency dye-sensitized solar cells. *Sol. Energy Mater. Sol. Cells* **2009**, *93*, 379–381.
11. Wang, Z.; Kawauchi, H.; Kashima, T.; Arakawa, H. Significant influence of TiO_2 photoelectrode morphology on the energy conversion efficiency of N719 dye-sensitized solar cell. *Coord. Chem. Rev.* **2004**, *248*, 1381–1389.
12. Zhao, Y.; Zhai, J.; Tan, S.; Wang, L.; Jiang, L.; Zhu, D. TiO_2 micro/nano-composite structured electrodes for quasi-solid-state dye-sensitized solar cells. *Nanotechnology* **2006**, *17*, 2090–2097.
13. Kim, Y.J.; Lee, M.H.; Kim, H.J.; Lim, G.; Choi, Y.S.; Park, N.; Kim, K.; Lee, W.I. Formation of highly efficient dye-sensitized solar cells by hierarchical pore generation with nanoporous TiO_2 spheres. *Adv. Mater.* **2009**, *21*, 3668–3673.
14. Sedghi, A.; Miankushki, H.N. Influence of TiO_2 electrode properties on performance of dye sensitized solar cells. *Int. J. Electrochem. Sci.* **2012**, *7*, 12078–12089.
15. Sahin, F.E.; Yılmaz, M. High concentration photovoltaics (HCPV) with diffractive secondary optical elements. *Photonics* **2019**, *6*, 68.
16. Ferber, J.; Luther, J. Computer simulations of light scattering and absorption in dye-sensitized solar cells. *Sol. Energy Mater. Sol. Cells* **1998**, *54*, 265–275.

17. Hore, S.; Vetter, C.; Kern, R.; Smit, H.; Hinsch, A. Influence of scattering layers on efficiency of dye-sensitized solar cells. *Sol. Energy Mater. Sol. Cells* **2006**, *90*, 1176–1188.
18. Nunomura, S.; Minowa, A.; Sai, H.; Knodo, M. Mie scattering enhanced near-infrared light response of thin-film silicon solar cells. *Appl. Phys. Lett.* **2010**, *97*, 063507.
19. Szygula, A.; Ruiz, M.; Sastre, A.; Guibal, E. Removal of an anionic reactive dye by chitosan and its regeneration. In Proceedings of the 2nd International Conference on WASTE MANAGEMENT, WATER POLLUTION, AIR POLLUTION, INDOOR CLIMATE (WWAI'08), Corfu, Greece, 26–28 October 2008.
20. Chen, A.-H.; Huang, Y.-Y. Adsorption of Remazol Black 5 from aqueous solution by the template crosslinked-chitosans. *J. Hazard. Mater.* **2010**, *177*, 668–675.
21. Tian, Z.; Tian, H.; Wang, X.; Yuan, S.; Zhang, J.; Zhang, X.; Yu, T.; Zou, Z. Multilayer structure with gradual increasing porosity for dye-sensitized solar cells. *Appl. Phys. Lett.* **2009**, *94*, 031905.
22. Son, M.K.; Seo, H.; Kim, S.K.; Hong, N.Y.; Kim, B.M.; Park, S.; Prabakar, K.; Kim, H.J. Analysis on the light-scattering effect in dye-sensitized solar cell according to the TiO_2 structural differences. *Int. J. Photoenergy* **2012**, *2012*, 480929.